Measured Delay and Doppler Profiles of Overtaking Vehicles at 60 GHz

Erich Zöchmann[1,2], Christoph F. Mecklenbräuker[2,3], Martin Lerch[1,2], Stefan Pratschner[1,2], Markus Hofer[4], David Löschenbrand[4], Jiri Blumenstein[3], Seun Sangodoyin[6], Gerald Artner[2], Sebastian Caban[1,2], Thomas Zemen[4], Aleš Prokeš[3], Markus Rupp[2,3], Andreas F. Molisch[6]

[1] Christian Doppler Laboratory for Dependable Wireless Connectivity for the Society in Motion,
[2] Institute of Telecommunications, TU Wien, Austria *ezoechma@nt.tuwien.ac.at*
[3] Department of Radio Electronics, TU Brno, Czech Republic
[4] Center for Digital Safety & Security, AIT Austrian Institute of Technology, Austria
[6] Wireless Devices and Systems Group, University of Southern California, USA

***Abstract*—We report results from real-world millimetre wave vehicle-to-vehicle channel measurements carried out in an urban street environment, down-town Vienna, Austria. Channel measurements have been acquired with a time-domain channel sounder in the frequency band 59.75–60.25 GHz with a frequency resolution of approximately 5 MHz. We estimate the local scattering function for sequential stationarity regions in time. A multitaper estimator is used to precisely define Doppler and delay resolutions. Estimates for delay and Doppler profiles are evaluated from the local scattering function for several overtaking vehicles at a variety of speeds and for different types of vehicles. The results show that passenger cars are associated with a single Doppler trajectory, whereas larger vehicles, such as trucks, show up in the data with multiple Doppler trajectories.**

***Index Terms*—mmWave, vehicular, propagation, measurement**

I. Introduction

The idea of assisted-driving or even self-driving cars is a game-changer of how people commute and therefore represents a tremendous attraction to both, industry and the research community. More then ten years ago, a first forward collision warning system based on a millimetre wave (mmWave) automotive radar was commercialized [1]. Nowadays, reliable mmWave communication systems, supporting the vehicle-to-vehicle information exchange, are supposed to be the next key enablers for the above mentioned assisted- or self-driving vehicles. Research of narrowband mmWave communication systems intended for vehicular application has been conducted for several decades. Meinel and Plattner [2] analyse a mmWave communication system for an infrastructure to train scenario already in 1983. Akihito et al. [3] investigate 60 GHz based car-to-car communications in 2001. Both works focus on path loss results and show two-ray fading [4], [5].

Due to recent advances in the technology of integrated circuits, broadband vehicular mmWave communications has gained interest [6]. The analysis of static mmWave channels is already well advanced, see for example [7]–[11]. For static environments frequency-domain channel sounding methods based on vector network analysers can be used [12]. However, for dynamic time-variant scenarios a time-domain channel sounding set-up is required, which was treated so far only by few research papers [13], [14]. In 2016, the authors of [15] evaluate the effect of vehicles' vibrations while in operation via delay-Doppler spreading functions with several GHz of bandwidth. A year later in [16], signal-to-noise ratio (SNR) fluctuations for 60 GHz transmissions with 5 MHz bandwidth in a vehicle-to-infrastructure scenario are investigated.

With this paper, we contribute to the dynamic mmWave vehicle-to-vehicle channel research in terms of: Firstly, introduction of a time-domain channel sounder design. Secondly, presentation of a wideband (500 MHz) time-domain mmWave channel measurement campaign performed in a real-world street environment. Thirdly, evaluation of delay and Doppler profiles for overtaking vehicles at a variety of speeds and for different vehicle types.

II. Scenario Description

Our receiver is fixed to the left rear car window, while our transmitter is mounted on a tripod approximately 15 m behind. We are observing the effect off passing/overtaking cars with excess speeds of up to $10\,\mathrm{m/s}$. Although we do not move our receiver and transmitter at all, it is still an accurate model of an overtaking process, since the Doppler relevant velocity is only given by the relative speed between the slower vehicles and a fast vehicle. Our case corresponds to a moving frame of reference. The transmitter (TX) and receiver (RX) placement is shown in Fig. 1. Double reflections at the transmitter car are below the receiver sensitivity. Hence, the transmitter car is omitted and replaced by a simpler tripod mounting. For our set-up the 60 GHz free space path loss calculates to 91.5 dB. At the transmit side a 20 dBi horn antenna is used and aligned to cover both the receiving car and the street, within the 3 dB opening angle. Surrounding buildings are filtered by the directive horn antenna. At the receive side, a less directional antenna such as an omni-directional $\lambda/4$ monopole antenna or an open-ended waveguide (OEW) antenna is used. Thereby, the reflected components of the overtaking car are not spatially filtered. The antenna gain including the cable losses is approximately -4 dBi for the monopole antenna and 2 dBi for the OEW.

III. Measurement Set-Up

The hardware set-up is illustrated in Fig. 2. Our transmitter consists of an arbitrary waveform generator (AWG), continuously repeating a baseband sounding sequence, once triggered.

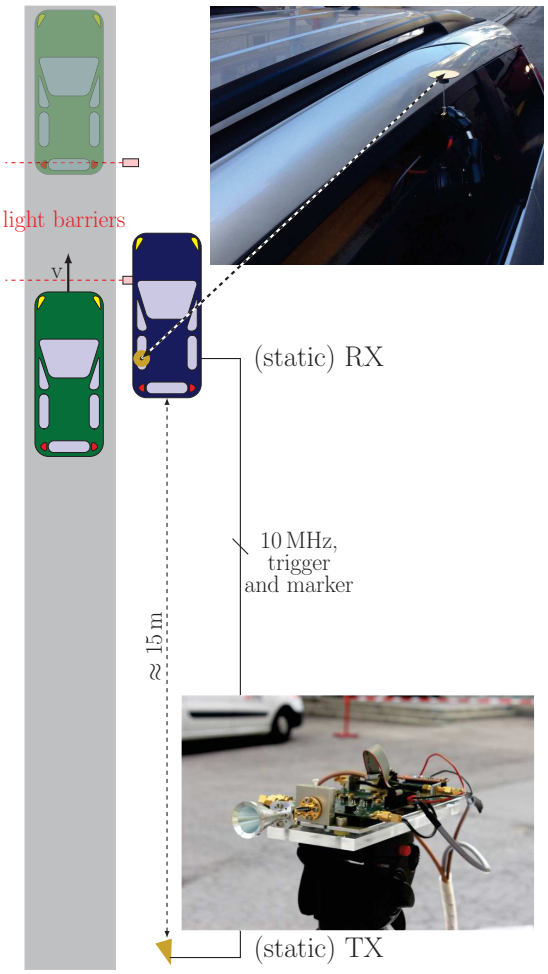

Fig. 1. Measurement scenario sketch.

This baseband sequence described in Sec. III-A is up-converted by an external mixer module. The external mixer module employs a synthesizer phase-locked loop (PLL) for generating the internal local oscillator (LO). The synthesizer PLL is fed by a 285.714 MHz reference, and uses a counter (divider) value of 210 to generate the center frequency of $f_0 = 59.99994\,\text{GHz}$. Our receiver is a Rohde and Schwarz signal analyser (SA) R&S FSW67. Its sensitivity is $P_{\text{SA,min}} = -150\,\text{dBm/Hz}$ at 60 GHz. All radio frequency (RF) devices are synchronized with a 10 MHz reference. A measurement is started when a vehicle passes through a first light barrier, triggering the AWG. The AWG itself plays out the baseband sequence and a sample synchronous marker. This marker signal triggers the recording of the receive samples. We directly access the IQ samples, sampled at a rate of 600 MSamples/s. A second light barrier, 3 m after the first one, is used to estimate the speed of passing vehicles.

A. Excitation Signal

The excitation signal generated by the AWG is a multi-tone waveform. The use of a multi-tone waveform affords us several advantages such as i) ideally, flat frequency spectrum, ii) design flexibility, iii) controllable crest factor, and iv) high

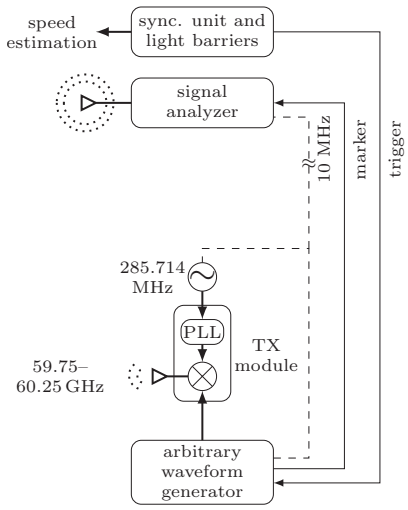

Fig. 2. Instruments sketch and their interplay.

SNR through processing gain. These advantages are important for channel transfer function extraction. Using an approach similar to a procedure implemented in [17], the excitation signal is given by $x(n) = \text{Re}\big(\sum_{k=1}^{K/2} \text{e}^{\text{j}\pi\frac{k^2}{K}} \text{e}^{-\text{j}2\pi k\frac{n}{Q}}\big)$, where $n = 0, \ldots, Q-1$ is the time index and k the sub-carrier index. To minimize the crest factor of the signal, the tone phases are chosen quadratic. The crest factor is reduced in order to maximize the average transmitted power while ensuring that all RF components encountered by the excitation signals operate in their linear regions.

For the geometry of our scenario, the length difference between the LOS and the overtaking car should always be smaller than 15 m. Ignoring multiple reflections between the parking RX car and the overtaking car, we can safely assume that the path length difference will not be larger than 30 m and thus 100 ns is our maximum excess delay. To make the symbols shorter and less susceptible to inter-carrier interference caused by phase noise and Doppler, we choose the sub-carrier spacing Δf as large as possible. To still obey the sampling theorem in the frequency domain, we need to fulfil $\Delta f \leq {}^{1}\!/_{2\tau_{\max}} = 5\,\text{MHz}$, where $\tau_{\max}$ is the maximum excess delay. Our multi-tone waveform has $Q = 121$ maximum available sub-carriers with a sub-carrier spacing $\Delta f = {}^{600\,\text{MHz}}\!/_{121} = 4.96\,\text{MHz}$. Due to the sharp (anti-aliasing) filter of the SA, from the $Q = 121$ sub-carriers we effectively utilize only $K = 102$ sub-carriers and a linearly interpolated zero DC sub-carrier, which is equal to a measurement bandwidth $B \approx 510.74\,\text{MHz}$. With these parameters the delay resolution of the channel sounder is $\tau_{\text{min}} = 1/B \approx 1.96\,\text{ns}$. The receiver sensitivity can be approximated to $P_{\text{RX,min}} = P_{\text{SA,min}} + 10\log_{10}(\Delta f) + 10\log_{10} K = -63\,\text{dBm}$.

B. Link budget and other limitations

For the LOS component, the propagation losses including antenna gains and 3 dB alignment margin sum up to $L = 78.5\,\text{dB}$. For the design of our set-up, we assume that reflected paths are $R = 10\,\text{dB}$ weaker than the LOS

TABLE I
CHANNEL SOUNDER PARAMETERS

Parameter	Value
sub-carrier spacing	$\Delta f = 4.96\,\text{MHz}$
number of sub-carriers	$K = 102$
center frequency	$f_0 = 59.99994\,\text{GHz}$
maximum alias free delay	$\tau_{\max} = 100.83\,\text{ns}$
transmit antenna	20 dBi conical horn
transmit power	$P_{\text{TX}} = 7\,\text{dBm}$
receiver sensitivity	$P_{\text{RX,min}} = -63\,\text{dBm}$
receive antenna	$\lambda/4$ monopole or OEW
snapshot rate	$T_{\text{snap}} = 129.1\,\mu\text{s}$
delay resolution	1.96 ns
maximum car speed	$v_{\text{car}} = 9.75\,\text{m/s}$
recording time	$T_{\text{rec}} = 720\,\text{ms}$

component. Next, we require an SNR at each sub-carrier of the reflected component of $\text{SNR}_{\text{refl}} = 10\,\text{dB}$. These requirements directly translate to the necessary transmit power $P_{\text{TX,min}} = P_{\text{RX,min}} + L + R + \text{SNR}_{\text{refl}} = 35.5\,\text{dBm}$. The maximum power for our transmit module is 7 dBm. Thus, the transmit power is 28.5 dB too low. The missing transmit power is realized by coherently averaging over $N = 640$ multi-tone symbols. Averaging over several symbols in time reduces the snapshot rate and limits the channel traceability. Remember, our multi-tone system has a sub-carrier spacing of $\Delta f = 4.96\,\text{MHz}$ and a sounding sequence length of $\tau_{\text{sym}} = 1/\Delta f = 202\,\text{ns}$. The overall pulse length including 640 repetitions, sums up to $T_{\text{snap}} = 129.1\,\mu\text{s}$. Applying the sampling theorem for the Doppler support, we obtain a maximum alias-free Doppler frequency of $\nu_{\max} = \frac{1}{2T_{\text{snap}}} = 3.9\,\text{kHz}$, which limits the speed of overtaking cars to $v_{\text{car}} = \lambda\nu_{\max}/2 = 9.75\,\text{m/s} = 35.1\,\text{km/h}$ [1]. This value is sufficient for our measurements, as the street, were the measurements took place, has a speed limit of 30 km/h. Our receiver is limited to a memory depth of approximately 420 MSamples or equivalently with a sampling rate of 600 MSamples/s we can record $T_{\text{rec}} = 720\,\text{ms}$ of the channel evolution. At 9.75 m/s this equals a driving distance of 7 m. An overview of the channel sounder parameters is given in Table I.

IV. MEASUREMENT EVALUATION

From the IQ samples we calculate the time-variant channel transfer function $H'[m', q]$ by a discrete Fourier transform of length $Q = 121$. Here m' denotes the symbol time index and q the frequency index. After averaging, we divide the resulting channel transfer function by the calibration function, obtained from back-to-back measurements, to equalize the frequency characteristics of the AWG to SA. The resulting function is denoted as $H[m, q]$, with $m = 0, \ldots, S-1$ denoting the resulting time index after averaging. For the measurement, we record $T_{\text{rec}} = 720\,\text{ms}$ which is equal to $S = 5579$ averaged snapshots.

We characterize the channel by the local scattering function (LSF) explained in [18]–[20]. We assume that the fading process is locally stationary within a region of M samples in time and $K+1$ (including a linearly interpolated zero sub-carrier at DC) samples in frequency domain. For a first evaluation we assume that there is only one stationarity region in the frequency direction. We estimate the LSF for consecutive stationarity regions in time. We use a multitaper based estimator in order to obtain multiple independent spectral estimates from the same measurement and being able to average them. The estimate of the LSF is defined as [18]

$$\hat{\mathcal{C}}[k_t; n, p] = \frac{1}{IJ} \sum_{w=0}^{IJ-1} \left| \mathcal{H}^{(G_w)}[k_t; n, p] \right|^2 . \tag{1}$$

We denote by $n \in \{0, \ldots, M-1\}$ the delay index and by $p \in \{-K/2, \ldots, K/2\}$ the Doppler index. The delay and Doppler shift resolutions are given by $\tau_s = 1/((K+1)\Delta f)$ and $\nu_s = 1/(MT_{\text{snap}})$. The time index of each stationarity region is $k_t \in \{0, \ldots, \lfloor S/M - 1 \rfloor\}$ and corresponds to the center of the stationarity regions. The windowed frequency response $\mathcal{H}^{(G_w)}$ is calculated by $\mathcal{H}^{(G_w)}[k_t; n, p] = \sum_{m=-M/2}^{M/2-1} \sum_{q=-K/2}^{K/2} H[m + M(k_t + 0.5), q] G_w[m, q] \mathrm{e}^{-\mathrm{j}2\pi(pm - nq)}$, where the tapers $G_w[m, q]$ are the discrete prolate spheroidal (DPS) sequences [21]. The number of tapers in time domain is $I = 3$ and in frequency domain $J = 3$.

For a first evaluation of the LSF we set $M = 117$ and $K + 1 = 103$ which corresponds to a stationarity region of $T_{\text{stat}} \approx 15.1\,\text{ms}$ in time and $B_{\text{stat}} \approx 510.74\,\text{MHz}$ in frequency. A more detailed investigation on the stationarity region length similar to [22] is ongoing. The power delay profile (PDP) and the Doppler spectral density (DSD) are calculated as a summation of the LSF over the Doppler or delay domain [18],

$$\hat{\mathcal{P}}_\tau[k_t; n] = E_p \left\{ \hat{\mathcal{C}}[k_t; n, p] \right\} = \frac{1}{M} \sum_{p=-M/2}^{M/2-1} \hat{\mathcal{C}}[k_t; n, p] , \tag{2}$$

$$\hat{\mathcal{P}}_\nu[k_t; p] = E_n \left\{ \hat{\mathcal{C}}[k_t; n, p] \right\} = \frac{1}{K} \sum_{n=0}^{K-1} \hat{\mathcal{C}}[k_t; n, p] , \tag{3}$$

where $E_i\{\cdot\}$ denotes the expectation with respect to i. In the measurement results we show the DSD and the PDP over time. For the evaluation a rectangular window is considered.

V. RESULTS

As a first example, we provide the DSD and the PDP of a single car. The car is shown in the upper part of Fig. 3. The transmitter height is $h_t = 1.1\,\text{m}$. As receiver, an omni-directional monopole antenna is used. In the middle part of Fig. 3, the PDP shows a strong static LOS component with 50 ns delay, corresponding to the 15 m distance, and a second delayed path which comes from the overtaking car. This second path produces the Doppler shift shown in the bottom part of Fig. 3. The second example is an overtaking convoy of two cars. All settings are equal to the first example. Both cars are visible as individual Doppler trajectories in Fig. 4. The last demonstrative example is an overtaking truck. The transmitter

[1] Remember, departing vehicles cause Doppler shifts twice as large.

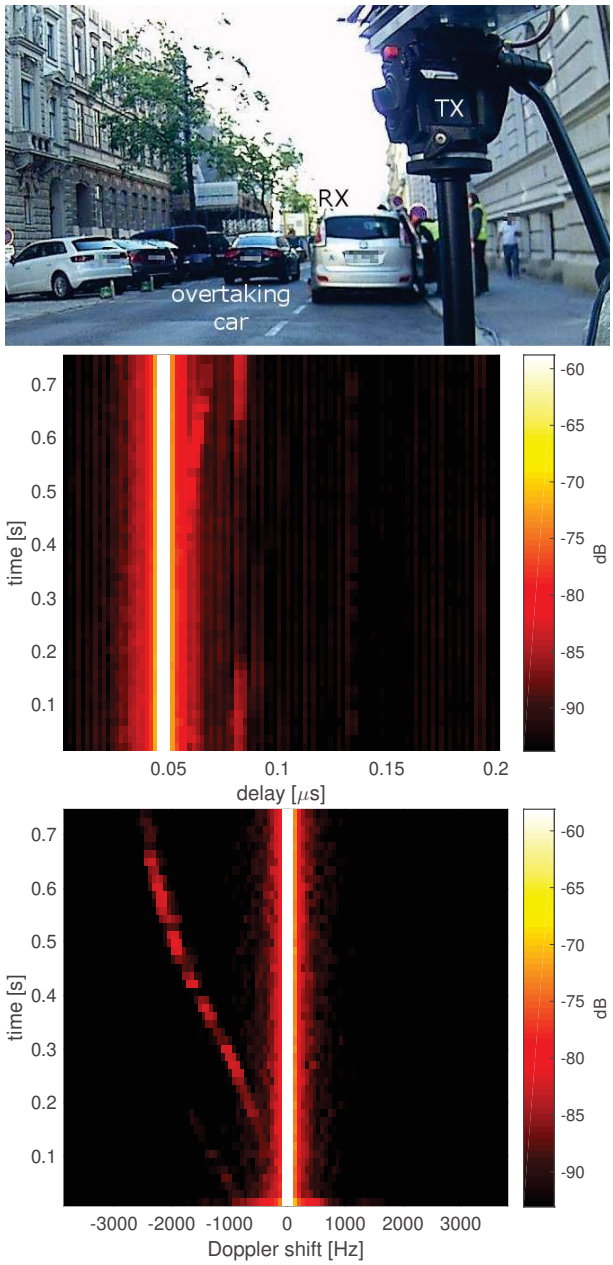

Fig. 3. One car scenario, $v = 7.3\,\mathrm{m/s}$. Top: Webcam snapshot. Middle: PDP. Bottom: DSD.

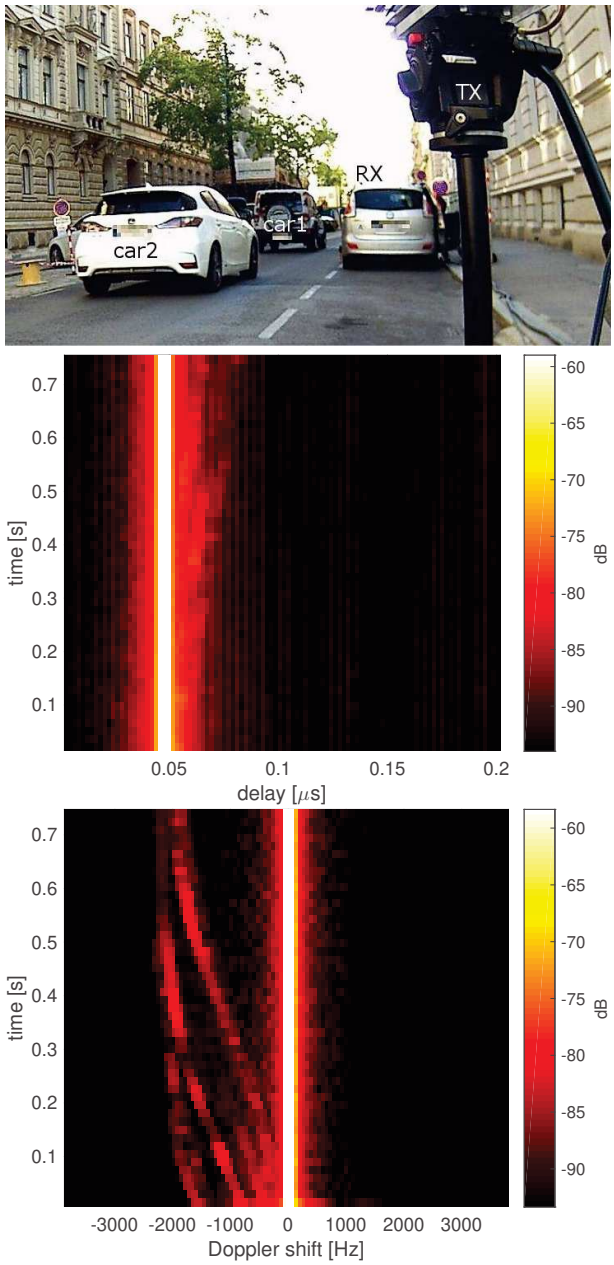

Fig. 4. Two cars scenario, $v = 5.9\,\mathrm{m/s}$. Top: Webcam snapshot. Middle: PDP. Bottom: DSD.

is now mounted at $h_t = 0.7\,\mathrm{m}$ and the receive antenna is changed to an OEW pointing towards the departing vehicles. Thereby, reflected components of departing cars are increased by the antenna gain. Due to the low transmitter mounting, a ground reflection is visible as second, strong and static component in the delay profile, shown in Fig. 5. The static ground reflection is an artefact due to the static TX and RX. Furthermore, cars parking in front of the RX are now also visible as distant reflection objects, vanishing once the truck drives by. Remarkably, the DSD looks very different from the previous examples. Besides the static Doppler component at $-3\,\mathrm{kHz}$ stemming from a distant car, the truck creates several Doppler traces, clearly demonstrating its spatial extend.

VI. Conclusion

We report empirical PDPs and DSDs from vehicular mmWave channel measurements in the 60 GHz band during September 2017. The channel measurements are characterized by estimates for the local scattering function and its marginal distributions. Different vehicles are distinguishable via their PDPs and DSDs. A passenger car results in a single multipath component, whereas a large vehicle such as a truck produces several multipath components.

Acknowledgment

The financial support by the Austrian Federal Ministry of Science, Research and Economy and the National Foundation for Research, Technology and Development is gratefully acknowledged. The research described in this paper was co-financed by the

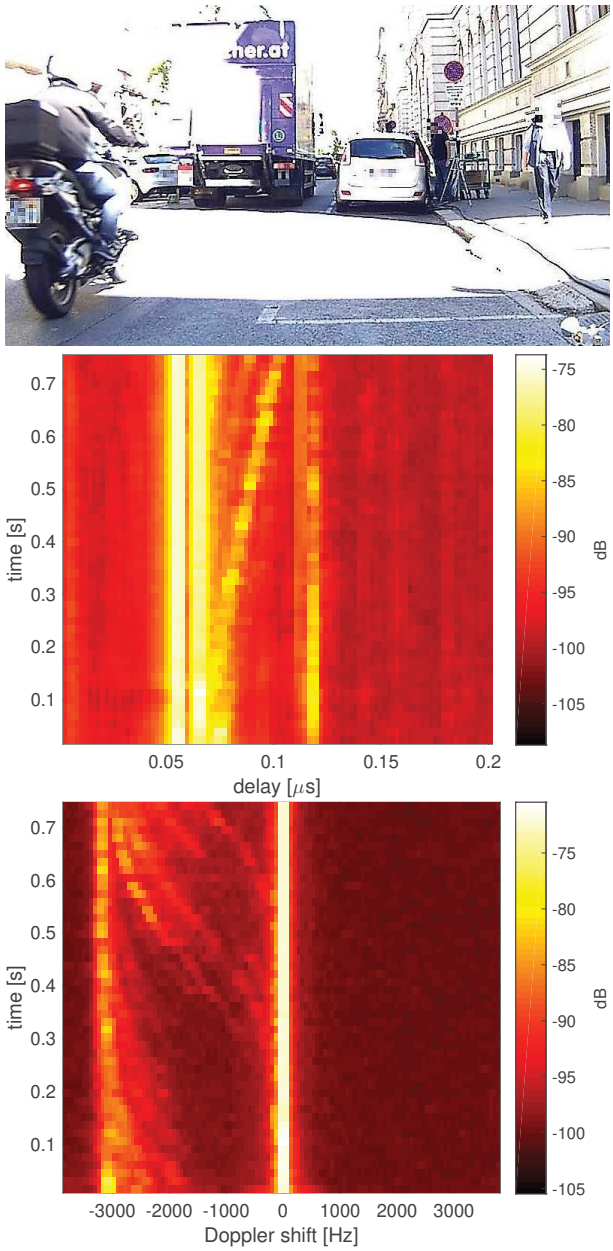

Fig. 5. Truck scenario, $v = 8\,\mathrm{m/s}$. Top: Webcam snapshot. Middle: PDP. Bottom: DSD.

Czech Science Foundation, Project No. 17-27068S and 17-18675S, and by National Sustainability Program under grant LO1401. For the research, the infrastructure of the SIX Center was used. This work was carried out in the framework of COST Action CA15104 IRACON.

REFERENCES

[1] T. Tokumitsu, M. Kubota, K. Sakai, and T. Kawai, "Application of GaAs device technology to millimeter-waves," *SEI Technical Review*, no. 79, pp. 57–65, 2014.

[2] H. Meinel and A. Plattner, "Millimetre-wave propagation along railway lines," *IEE Proceedings F (Communications, Radar and Signal Processing)*, vol. 130, no. 7, pp. 688–694, 1983.

[3] K. Akihito, S. Katsuyoshi, M. Fujise, and S. Kawakami, "Propagation characteristics of 60-GHz millimeter waves for ITS inter-vehicle communications," *IEICE Transactions on Communications*, vol. 84, no. 9, pp. 2530–2539, 2001.

[4] S. Takahashi, A. Kato, K. Sato, and M. Fujise, "Distance dependence of path loss for millimeter wave inter-vehicle communications," *Radio-engineering*, vol. 13, no. 4, p. 9, 2004.

[5] A. Yamamoto, K. Ogawa, T. Horimatsu, A. Kato, and M. Fujise, "Path-loss prediction models for intervehicle communication at 60 GHz," *IEEE Transactions on Vehicular Technology*, vol. 57, no. 1, pp. 65–78, 2008.

[6] V. Va, T. Shimizu, G. Bansal, and R. W. Heath Jr, "Millimeter wave vehicular communications: A survey," *Foundations and Trends® in Networking*, vol. 10, no. 1, pp. 1–113, 2016.

[7] E. Zöchmann, M. Lerch, S. Caban, R. Langwieser, C. F. Mecklenbräuker, and M. Rupp, "Directional evaluation of receive power, Rician K-factor and RMS delay spread obtained from power measurements of 60 GHz indoor channels," in *Proc. of IEEE-APS Topical Conference on Antennas and Propagation in Wireless Communications (APWC)*, 2016.

[8] J. Vehmas, J. Jarvelainen, S. L. H. Nguyen, R. Naderpour, and K. Haneda, "Millimeter-wave channel characterization at Helsinki airport in the 15, 28, and 60 GHz bands," in *Proc. of IEEE Vehicular Technology Conference (VTC-Fall)*, 2016.

[9] F. Fuschini, S. Häfner, M. Zoli, R. Müller, E. M. Vitucci, D. Dupleich, M. Barbiroli, J. Luo, E. Schulz, V. Degli-Esposti, and R. S. Thomä, "Analysis of in-room mm-Wave propagation: Directional channel measurements and ray tracing simulations," *Journal of Infrared, Millimeter, and Terahertz Waves*, vol. 38, no. 6, pp. 727–744, 2017.

[10] E. Zöchmann, M. Lerch, S. Pratschner, R. Nissel, S. Caban, and M. Rupp, "Associating spatial information to directional millimeter wave channel measurements," in *Proc. of IEEE Vehicular Technology Conference (VTC2017-Fall)*, 2017, pp. 1–5.

[11] J. Blumenstein, A. Prokeš, A. Chandra, T. Mikulasek, R. Marsalek, T. Zemen, and C. Mecklenbräuker, "In-vehicle channel measurement, characterization, and spatial consistency comparison of 30–11 GHz and 55–65 GHz frequency bands," *IEEE Transactions on Vehicular Technology*, vol. 66, no. 5, pp. 3526–3537, May 2017.

[12] A. Chandra, A. Prokeš, T. Mikulasek, J. Blumenstein, P. Kukolev, T. Zemen, and C. F. Mecklenbräuker, "Frequency-domain in-vehicle UWB channel modeling," *IEEE Transactions on Vehicular Technology*, vol. 65, no. 6, pp. 3929–3940, June 2016.

[13] P. B. Papazian, C. Gentile, K. A. Remley, J. Senic, and N. Golmie, "A radio channel sounder for mobile millimeter-wave communications: System implementation and measurement assessment," *IEEE Transactions on Microwave Theory and Techniques*, vol. 64, no. 9, pp. 2924–2932, 2016.

[14] E. Zöchmann, S. Caban, M. Lerch, and M. Rupp, "Resolving the angular profile of 60 GHz wireless channels by delay-Doppler measurements," in *Proc. of IEEE Sensor Array and Multichannel Signal Processing Workshop (SAM)*, 2016, pp. 1–5.

[15] J. Blumenstein, J. Vychodil, M. Pospisil, T. Mikulasek, and A. Prokeš, "Effects of vehicle vibrations on mm-wave channel: Doppler spread and correlative channel sounding," in *Proc. of IEEE International Symposium on Personal, Indoor, and Mobile Radio Communications (PIMRC)*, Sept 2016, pp. 1–5.

[16] A. Loch, A. Asadi, G. H. Sim, J. Widmer, and M. Hollick, "mm-wave on wheels: Practical 60 GHz vehicular communication without beam training," *Proc. of COMSNETS 2017*, pp. 1–5, 2017.

[17] S. Sangodoyin, J. Salmi, S. Niranjayan, and A. F. Molisch, "Real-time ultrawideband MIMO channel sounding," in *Proc. of Antennas and Propagation Conference (EUCAP)*, 2012.

[18] L. Bernadó, T. Zemen, F. Tufvesson, A. F. Molisch, and C. F. Mecklenbräuker, "Delay and Doppler Spreads of Nonstationary Vehicular Channels for Safety-Relevant Scenarios," *IEEE Transactions on Vehicular Technology*, vol. 63, no. 1, pp. 82–93, Jan. 2014.

[19] L. Bernadó, T. Zemen, F. Tufvesson, A. F. Molisch, and C. F. Mecklenbräuker, "Time- and Frequency-Varying K -Factor of Non-Stationary Vehicular Channels for Safety-Relevant Scenarios," *IEEE Transactions on Intelligent Transportation Systems*, vol. 16, no. 2, pp. 1007–1017, 2015.

[20] D. J. Thomson, "Spectrum estimation and harmonic analysis," *Proceedings of the IEEE*, vol. 70, no. 9, pp. 1055–1096, 1982.

[21] D. Slepian, "Prolate Spheroidal Wave Functions, Fourier Analysis, and Uncertainty-V: The Discrete Case," *Bell System Technical Journal*, vol. 57, no. 5, pp. 1371–1430, May 1978.

[22] L. Bernadó, T. Zemen, F. Tufvesson, A. F. Molisch, and C. F. Mecklenbräuker, "The (in-) validity of the WSSUS assumption in vehicular radio channels," in *Proc. of IEEE International Symposium on Personal, Indoor and Mobile Radio Communications (PIMRC)*, Sept 2012, pp. 1757–1762.